**ONLINE SUPPLEMENT**

# Distinct roles of myofibroblast-specific Smad2 and Smad3 signaling in repair and remodeling of the infarcted heart

Shuaibo Huang[1], Bijun Chen[1], Ya Su[1], Linda Alex[1], Claudio Humeres[1], Arti V Shinde[1], Simon J Conway[2], and Nikolaos G Frangogiannis[1]

Short title: Smad2 and Smad3 in infarct myofibroblasts

[1]The Wilf Family Cardiovascular Research Institute, Department of Medicine (Cardiology), Albert Einstein College of Medicine, Bronx NY; [2]Department of Pediatrics, Indiana University, Indianapolis IN.

## SUPPLEMENTARY METHODS

**Generation of mice with myofibroblast-specific loss of Smad2**: In order to study the role of Smad2 in fibroblasts in the infarcted myocardium, we generated mice with loss of Smad2 in activated infarct fibroblasts (FS2KO). We used a transgenic mouse line in which Cre recombinase was driven by a 3.9-kb mouse *Postn* promoter[1,2]. Periostin, which is encoded by *Postn*, is not expressed in cardiomyocytes, vascular cells, hematopoietic cells or quiescent cardiac fibroblasts[3,4], but is upregulated in injury site myofibroblasts in infarcted and in pressure-overloaded hearts [4,5]. Postn-Cre mice (in a C57Bl6J background) were bred with Smad2 fl/fl mice (The Jackson Laboratory, Stock No: 022074) to generate Postn-Cre;Smad2 fl/fl animals (FS2KO) and corresponding Smad2 fl/fl controls. 55 Smad2 fl/fl mice (M, n=32, F, n=23) and 57 FS2KO animals (M, n=33, F, n=24) underwent in vivo experimentation. Material from previously published[6] mice with myofibroblast-specific loss of Smad3 (FS3KO) and corresponding Smad3 fl/fl mice undergoing infarction protocols was used to compare the effects of myofibroblast-specific Smad2 and Smad3 loss.

**Mouse model of non-reperfused myocardial infarction**: Animal studies were approved by the Institutional Animal Care and Use Committee at Albert Einstein College of Medicine and conform with the Guide for the Care and Use of Laboratory Animals published by the National Institutes of Health. A mouse model of non-reperfused myocardial infarction was used, as previously described by our group[6]. Female and male mice, 4-6 months of age, were anesthetized using inhaled isoflurane (2%). All Smad2 fl/fl, Smad3 fl/fl, FS2KO, and FS3KO mice used for in vivo experiments were from our own colonies. For analgesia, buprenorphine (0.05-0.2 mg/kg s.c) was administered at the time of surgery and q12h thereafter for 2 days. Additional doses of analgesics were given if the animals appeared to be experiencing pain (based on criteria such as immobility and failure to eat). Intraoperatively, heart rate, respiratory rate and electrocardiogram were continuously monitored and the depth of anesthesia was assessed using the toe pinch method. To assess the time-course of activation of Smad2 and Smad3 signaling in the infarct heart, the left anterior descending (LAD) coronary artery of

C57/BL6J WT mice was permanently occluded for 24h, 3d, 7d, and 28d. To assess cardiac function and remodeling following myocardial infarction, animals underwent echocardiographic analysis at baseline and 7 days, 28 days after permanent coronary occlusion (Baseline: Smad2 fl/fl, M, n=18, F, n=19, FS2KO, M, n=16, F, n=22; 7 days, Smad2 fl/fl, M, n=19, F, n=17; FS2KO, M, n=18, F, n=19; 28 days, Smad2 fl/fl, M, n=6, F, n=11; MFS2KO, M, n=8, F, n=15). At the end of the experiment, euthanasia was performed using 2% inhaled isoflurane followed by cervical dislocation. Early euthanasia was performed with the following criteria, indicating suffering of the animal: weight loss>20%, vocalization, dehiscent wound, hypothermia, clinical signs of heart failure (cyanosis, dyspnea, tachypnea), lack of movement, hunched back, ruffled coat, lack of food or water ingestion.

**Echocardiograph**y: Echocardiographic studies were performed before instrumentation, 7 and 28 days after coronary occlusion using the Vevo 2100 system (VisualSonics. Toronto ON), as previously described [7]. Parasternal long-axis (PSLAX) M-mode was used for measurement of systolic and diastolic ventricular and wall diameters. PSLAX IVS tool was used to measure and calculate the thickness of the intraventricular septum (IVS-d and IVS-s), left ventricular posterior wall (PWTh-d and PWTh-s), the left ventricular end-diastolic internal dimension (LVID-d), left ventricular end-systolic internal dimension (LVID-s), and the ratio of left ventricular mass/body weight (LVM/BW). Left ventricular end-diastolic volume (LVEDV), left ventricular end-systolic volume (LVESV) were measured as indicators of dilative remodeling. Left ventricular ejection fraction (LVEF= [(LVEDV－LVESV) / LVEDV] ×100%), fractional shortening (FS = [(LVID-d – LVID-s) / LVID-d] ×100%) were measured for assessment of systolic ventricular function.

**Immunohistochemistry and histology**: For histopathological analysis murine hearts were fixed in zinc-formalin (Z-fix; Anatech, Battle Creek, MI), and embedded in paraffin. Infarcted hearts were sectioned from base to apex at 250 μm intervals, thus reconstructing the whole heart, as previously described [8]. 20 sections (5μm thick) were cut at each level. The first section at each partition was stained with haematoxylin and eosin (H&E). Morphometric parameters were quantitatively assessed using Axiovision software. The infarcted and

non-infarcted areas were measured at each level and the volume of the infarct and of the non-infarcted remodeling myocardium at each level was calculated as: Infarct volume= infarct area X 350μm (250μm + 20 sections*5μm=350μm), and volume of non-infarcted remodeling myocardium=non-infarcted area X 350μm. The total volume of the infarcted and non-infarcted myocardium was calculated as the sum of the volumes of each partition. Scar size was measured by dividing the volume of the infarct to the total volume of the left ventricle (infarct volume+volume of non-infarcted myocardium), and was expressed as a percentage. Minimum and maximum wall thickness of both infarcted and non-infarcted left ventricular segments was measured using Axiovision software. In order to assess collagen content, 3 sections from each heart (representing the basal, mid-myocardial and apical levels) were stained with picrosirius red to label the collagen fibers. 8-10 fields from the infarcted and remote non-infarcted remodeling myocardium were scanned and the collagen-stained area was measured. Collagen content was measured in the infarct region, and in the remote remodeling myocardium using ImagePro software as the ratio of the collagen stained area to the total area and was expressed as a percentage for reach animal.

**Dual immunofluorescence:** In order to detect Smad2 and Smad3 activation in activated fibroblasts, we performed dual immunofluorescence for pSmad2 (using an anti-pSmad2 antibody, Invitrogen, 44-244G), or pSmad3 (anti-pSmad3 antibody, Invitrogen, PA5-37636) and α-smooth muscle actin (anti α-SMA antibody, Sigma, F3777). Activation of Smad2 or Smad3 signaling was evidenced by nuclear localization of pSmad2 or pSmad3. Myofibroblasts were identified by staining with FITC conjugated anti-α-smooth muscle actin (FITC-α-SMA) (Sigma, F3777), or by staining with an antibody to periostin (NOVUS Biologicals, AF2955) as spindle-shaped cells located outside the vascular media. Endpoints reflecting myofibroblast size, shape, alignment and polarization were assessed using ImagePro software as previously described[6]. The ratio of major to minor axis of infarct myofibroblasts was calculated to assess the myofibroblast morphology. To quatitatively assess myofibroblast alignment in the healing infarcts, angle between the long axis and the tangent of the ventricular wall (indicated by a red arrow in Figure 6) was measured. Characteristics of myofibroblast

morphology and polarization were assessed in 3-9 animals from each group, at 2 different levels. 6 fields were quantified in each animal. A total of 18 cells from each animal was assessed to perform statistical analysis. In order to compare the density of α-SMA+ myofibroblasts, myofibroblast numbers were assessed in 6 fields in each animal from 2 different levels (S2fl/fl, n=3, FS2KO, n=4, S3fl/fl, n=9, FS3KO, n=5). To document the loss of Smad2 in infarct myofibroblasts, dual staining with the Goat anti-Periostin (NOVUS Biologicals, AF2955) and Rabbit anti-Smad2 (Cell Signaling Technology, 5339) antibodies was used in the sections of S2fl/fl and FS2KO, followed by Alexa Fluor 594 (Invitrogen, A21207) and Alexa Fluor 488–conjugated secondary antibodies (Invitrogen, A21206) respectively. All sections were counterstained with DAPI. Quantitative analysis was performed by counting the number of periostin+ Smad2+ and periostin+ Smad2- cells in 5 fields from 2 different sections from each animal (S2fl/fl, n=4, FS2KO, n=5).

**Isolation and stimulation of isolated cardiac fibroblasts**: Fibroblasts were isolated from normal mouse (C57/BL6J) hearts as previously described [9],[10], then cultured in dishes (Corning, Cat#: 353003, Falcon® 100 mm X15 mm), or in collagen pads. For experiments examining effects of TGF-β superfamily ligands on Smad2 activation, cells plated in dishes were stimulated with TGF-β1 (10ng/ml), TGF-β2 (10ng/ml), TGF-β3 (10ng/ml), BMP2 (50ng/ml), BMP4 (50ng/ml), BMP7 (50ng/ml), Angiotensin II (50ng/ml) (all from R&D Systems) for 30 minutes. At the end of the experiment fibroblast lysates were used for protein extraction.

siRNA KD experiments were performed in fibroblasts cultured in collagen pads (to assess integrin expression), or in fibroblasts cultured in plates (to assess planar cell polarity genes). Mouse cardiac fibroblasts at passage 1 were seeded at 80% confluence (100 mm dishes) in Dulbecco's modified eagle medium (DMEM) and were either transfected with 50 nM ON-TARGET plus mouse Smad2 siRNA, Smad3 siRNA or transfected with a non-silencing control siRNA (Dharmacon) using Lipofectamine® 3000 Reagent (ThermoFisher Scientific). The ON-TARGET modification is shown to dramatically decrease the off-target effects of the siRNA. The cells were returned to a 5% CO2 incubator and allowed to recover for 24 h. After 24h, the cells were harvested using

TrypLE ™ Express reagent, counted and populated on collagen pads (3 $\times 10^5$ cells/ml concentration). The pads were then suspended in serum free DMEM/F12 for an additional 72 h.

In additional experiments designed to assess planar cell polarity (PCP) pathway genes, fibroblasts cultured in dishes were transfected with control, Smad2 or Smad3 siRNA for 72h in DMEM/F12 with 10% FBS. Afterwards, cells were rinsed twice with DPBS, and then 1 mL Trizol solution was added in each dish for cell lysis and RNA extraction. Extracted RNA was used for PCR array analysis.

**RNA extraction, qPCR and qPCR array analysis**: Total RNA was extracted from cells, cDNA was amplified using the SsoFast EvaGreen Supermix reagent and the C1000 thermal cycler apparatus from Bio-Rad following the manufacturer's recommendations. The following primer pairs were used: GAPDH forward 5'-AGGTCGGTGTGAACGGATTTG-3', GAPDH reverse 5'-TGTAGACCATGTAGTTGAGGTCA-3', α-SMA forward 5'-GTCCCAGACATCAGGGAGTAA-3', α-SMA reverse 5'-TCGGATACTTCAGCGTCAGGA-3', Smad2 forward 5'-ATCTTGCCATTCACTCCGCC-3', Smad2 reverse 5'-TCTGAGTGGTGATGGCTTTCTC -3', Smad3 forward 5'-CACGCAGAACGTGAACACC-3', Smad3 reverse 5'-GGCAGTAGATAACGTGAGGGA-3', Itga2 forward 5'-GCACCACATTAGCATACA-3', Itga2 reverse 5'-TAGAAAGGGATACTGAAGACT-3', Itga5 forward 5'-AGTGTGAGGCTGTATATGA-3', Itga5 reverse 5'-AGAATGGCTAGGATGATGA-3', NOX2 forward 5'-ATCCATATCCGTATTGTG-3', NOX2 reverse 5'-ATCAACTGCTATCTTAGG-3', periostin forward 5'-AACCTGGATTCTGACATT -3', periostin reverse 5'-GTACATTGAAGGAATAACCAT -3'. vimentin forward 5'-CGTCCACACGCACCTACAG-3' , vimentin reverse 5'-GGGGGATGAGGAATAGAGACT-3'. The housekeeping gene GAPDH was used as internal control. The qPCR procedure was repeated three times in independent runs; gene expression levels were calculated using the ΔΔCT method.

In order to assess gene expression of planar cell polarity (PCP) pathway genes, we used a PCR array. Fibroblasts cultured in DMEM/F12 with 10% FBS were transfected with siRNA for 72h and then cells were harvested for RNA extraction using Trizol. A total of 400ng RNA was reverse-transcribed into cDNA using the

$RT^2$ first strand kit (Qiagen, 330404). Quantitative PCR was performed using the $RT^2$ Profiler mouse WNT signaling pathway PCR array (PAMM-043ZA) from Qiagen according to manufacturer's protocol. The same thermal profile conditions were used for all primers sets: 95℃ for 10 minutes, 40 cycles at 95℃ for 15 seconds followed at 60℃ for 1 minute. The data obtained were exported to SABiosciences PCR array web-based template where it was analyzed using the ΔΔCT method.

**Protein extraction and western blotting**: Protein was extracted from cardiac fibroblasts as previously described [11]. Halt™ Phosphatase Inhibitor Cocktail (Thermo Scientific™, 78420) was used to preserve the phosphorylation state of proteins during and after cell lysis or protein extraction. Western blotting was performed using antibodies to pSmad2 [$pSpS^{465/467}$] (Cell Signaling Technology, 3108), Smad2 (Cell Signaling Technology, 5339), and GAPDH (Santa Cruz, 25778). The gels were imaged by ChemiDoc™ MP System (Bio Rad) and analyzed by Image Lab 3.0 software (Bio Rad).

**Assessment of α-SMA incorporation into the cytoskeleton of stimulated cardiac fibroblasts**: To assess the effects of Smad2 or Smad3 loss on myofibroblast conversion, fibroblasts were treated with control, Smad2 or Smad3 siRNA for 72h. Specific reduction of Smad2 and Smad3 expression was documented using qPCR. Dual fluorescence with phalloidin-AF594 (Invitrogen, A12381) and anti-α-SMA-FITC-labeled antibody (Sigma, F3777) was used to assess decoration of F-actin fibers with α-SMA in fibroblasts cultured in chamber slides in the presence or absence of TGF-β1 (10ng/ml, 72h). The density of phalloidin+/α-SMA+ fibroblasts was counted in 4 chamber slides of each group. 5 fields were quantified in each chamber slide and the percentage of α-SMA+/phalloidin+ cells to the total number of phalloidin+ cells was used to quantify α-SMA incorporation into the cytoskeleton.

**Fibroblast migration assay:** Cardiac fibroblast migration assay was performed using colorimetric transwell system QCMTM 24-Well (Millipore Corporation, Billerica, MA), which allows cells to migrate through an 8-μm pore size polycarbonate membrane. Fibroblasts were treated with control, Smad2 or Smad3 siRNA for 72h when cells grew up to 80% confluence, followed by serum starvation for 24h prior to migration assay. Then

cells were harvested with TrypLE express (GIBCO Invitrogen Corporation, Carlsbad, CA), counted and reconstituted with serum free DMEM/F12 (GIBCO Invitrogen Corporation, Carlsbad, CA) to bring the cells to concentration of 1.0X106 cells/ml. Subsequently, 300µl fibroblasts suspensions were added into the upper chamber of each insert, and 500 µl serum free DMEM/F12, or 1% FBS DMEM/F12 with 20 ng/ml TGF-β1 were added in the lower chamber, The chambers were incubated for 6 h at 37$^{o}$C in 5% CO2. After incubation remaining cells/media from the top side of the insert were removed by pipetting, and the migration insert was placed into a clean well containing 400 µL of Cell Stain (crystal violet) for 20 min at room temperature. Afterwards, inserts were rinsed in distilled water. Migrated cells were visualized and photographed using an inverted microscope, and cell migration was quantified by counting cells in 5 random high power fields (40X). Dry inserts were transferred to extraction buffer and placed on rocking platform for 15 min. Optical density of dye extract was measured at 560 nm using a plate reader (BioTek).

**Statistics**: For comparisons of two groups unpaired, 2-tailed Student's t-test using (when appropriate) Welch's correction for unequal variances was performed. The Mann-Whitney test was used for comparisons between 2 groups that did not show Gaussian distribution. For comparisons of multiple groups, 1-way ANOVA was performed followed by Tukey's multiple comparison test. The Kruskall-Wallis test, followed by Dunn's multiple comparison post-test was used when one or more groups did not show Gaussian distribution. Survival analysis was performed using the Kaplan-Meier method. Mortality was compared using the log rank test.

## SUPPLEMENTARY FIGURES:

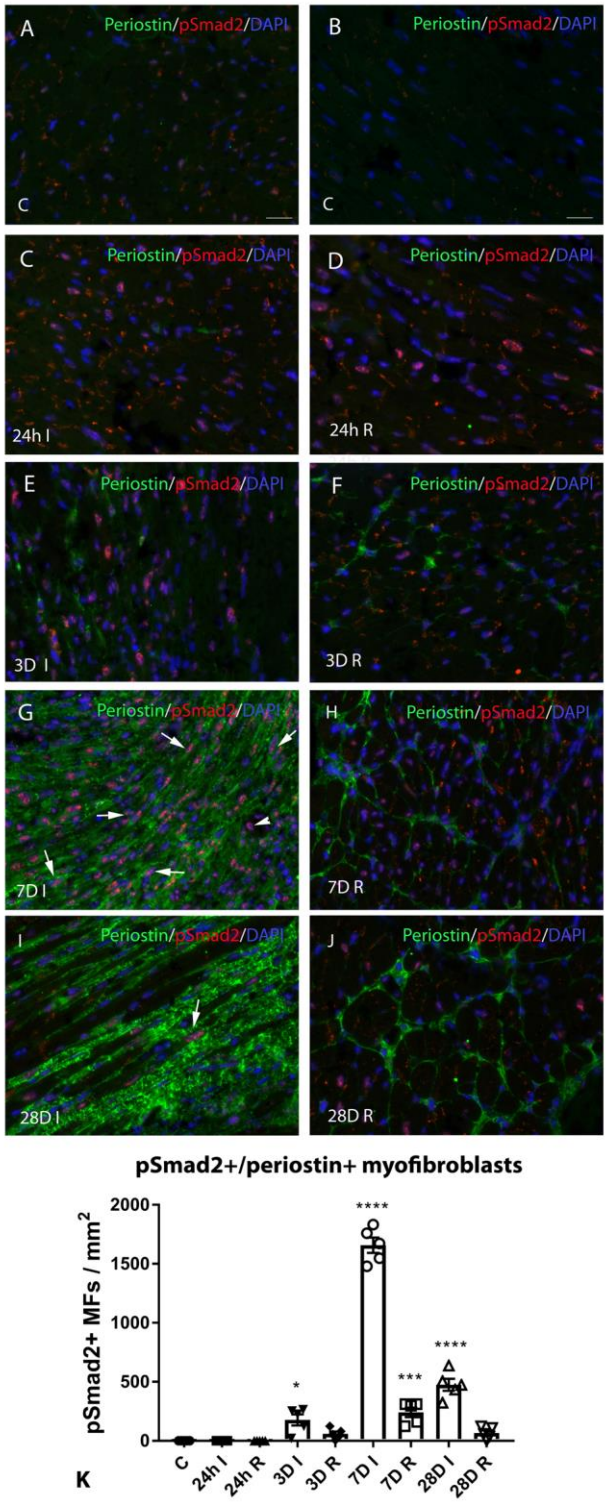


**Supplemental Figure I**: **Smad2 activation in periostin-expressing myofibroblasts infiltrating the infarcted myocardium.** Dual immunofluorescence for periostin and pSmad2 was performed in control hearts (A-B) and in infarcted (I) and non-infarcted remote (R) myocardial segments from mice undergoing 24h (C-D), 3-day (E-

F), 7-day (G-H) and 28-day (I-J) coronary occlusion protocols. Control (Con) hearts (A-B) showed no periostin immunoreactivity and low levels of pSmad2 expression. High levels of pSmad2 immunoreactivity were noted in abundant periostin+ myofibroblasts infiltrating the infarcted myocardium after 7 days of coronary occlusion (arrows). Periostin+/pSmad2+ cells were rare after 28 days of coronary occlusion (arrow). Please note deposition of periostin in the extracellular matrix in both infarcted (G, I) and remote remodeling segments (H, J) after 7-28 days of coronary occlusion. K: Quantitative analysis showed an early increase in the density of pSmad2+ periostin-expressing myofibroblasts after 3 days of coronary occlusion, followed by a peak after 7 days (*$p<0.05$, ***$p<0.001$, ****$p<0.0001$ vs. control, n=5/group). Increased density of pSmad2+ myofibroblasts was noted in the remodeling non-infarcted myocardium after 7 days of coronary occlusionStatistical analysis was performed using ANOVA followed by Tukey's multiple comparison test.

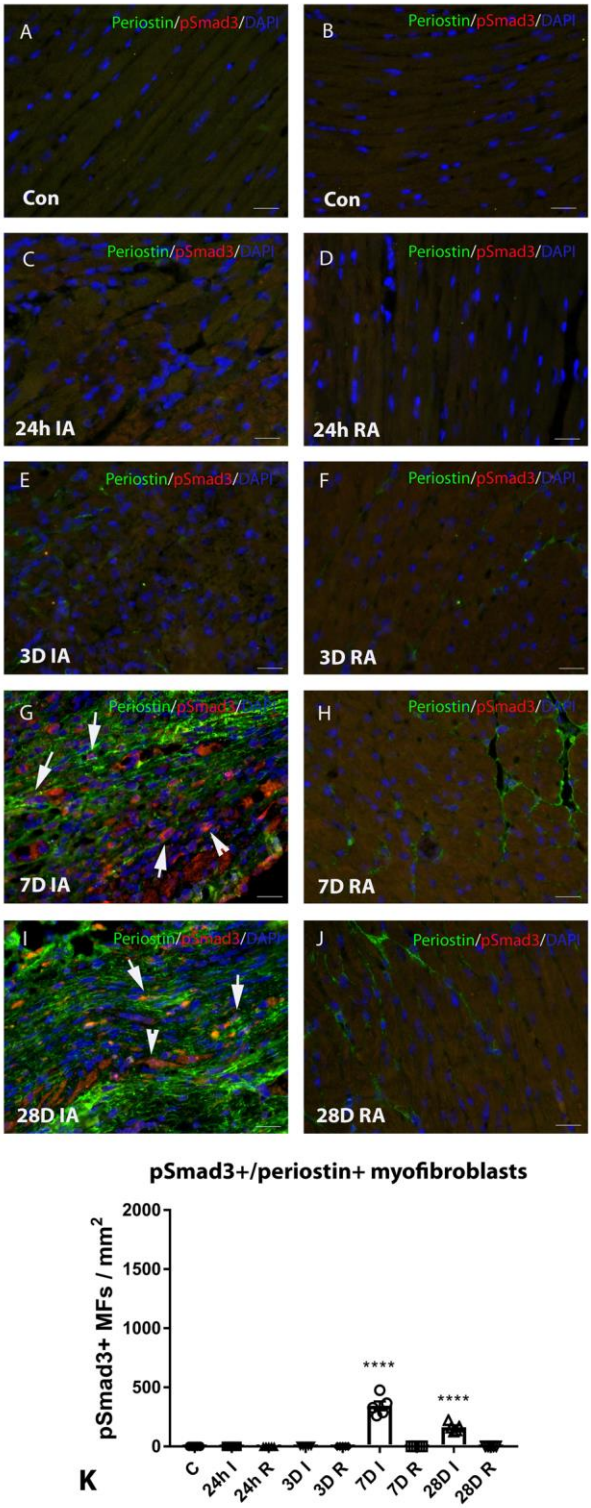


**Supplemental figure II**: **Smad3 activation in periostin-expressing infarct myofibroblasts**. Dual immunofluorescence for periostin and pSmad3 was performed in control hearts (A-B) and in infarcted (I) and non-infarcted remote (R) myocardial segments from mice undergoing 24h (C-D), 3-day (E-F), 7-day (G-H) and

28-day (I-J) coronary occlusion protocols. Control (Con) hearts (A-B) and infarcted heart at 24h timepoint (C-D) showed no periostin immunoreactivity or pSmad3 expression. Expression of pSmad3 was noted in periostin+ myofibroblasts infiltrating the infarcted myocardium after 7 days (G-H) and 28 days (I-J) of coronary occlusion (arrows). Please note deposition of periostin in the extracellular matrix in both infarcted (G, I) and remote remodeling segments (H, J) after 7-28 days of coronary occlusion. K: Quantitative analysis showed that Smad3 activation in periostin-expressing myofibroblasts peaked after 7 days of coronary occlusion (****$p<0.0001$ vs. control, n=5/group). Statistical analysis was performed using ANOVA followed by Tukey's multiple comparison test.

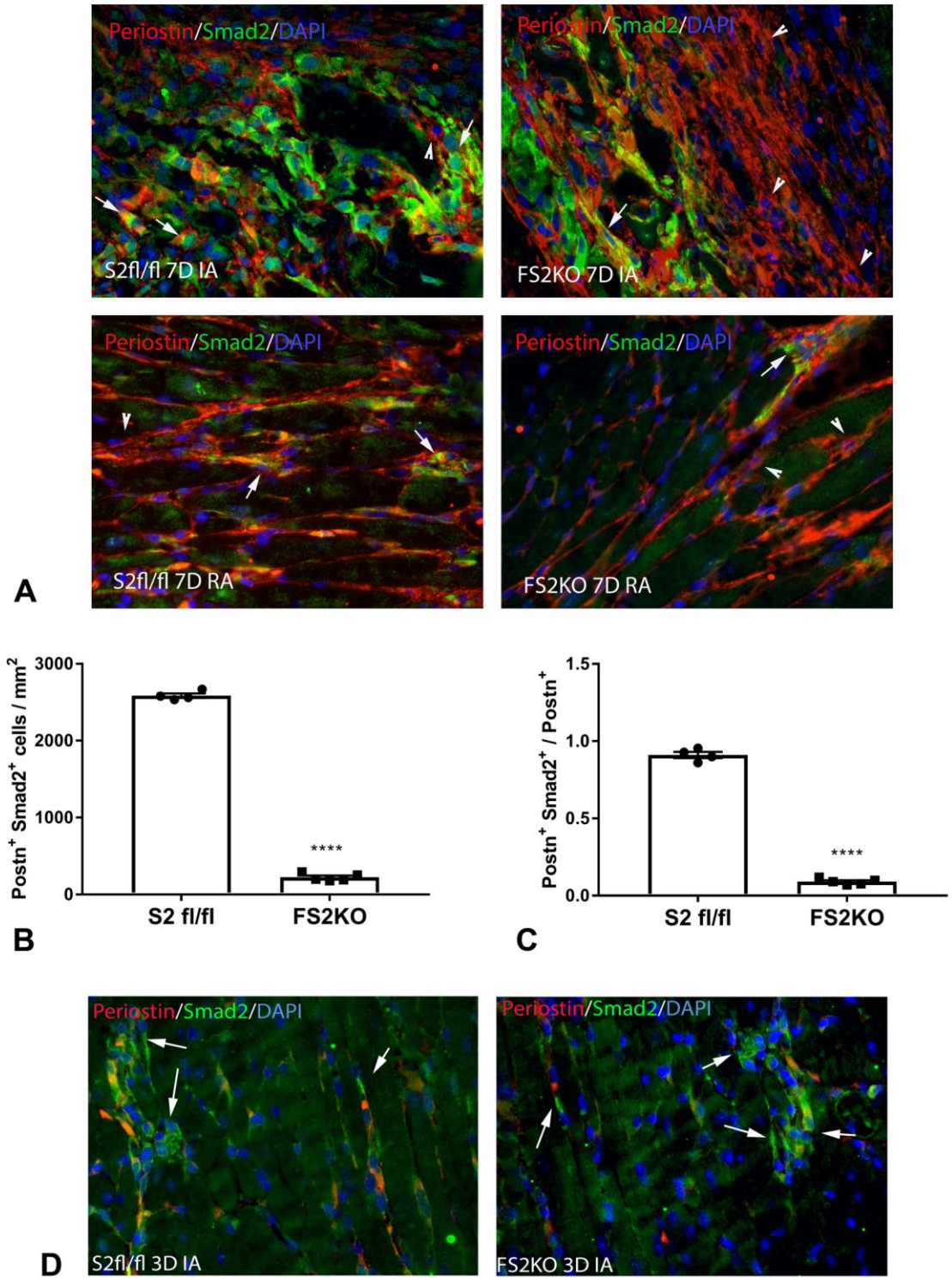


**Supplemental Figure III**: **FS2KO mice have reduced Smad2 expression in periostin+ myofibroblasts after 7 days of coronary occlusion**. A: In order to document myofibroblast-specific Smad2 loss, dual immunofluorescence for Smad2 and periostin was performed in Smad2 fl/fl and FS2KO mouse hearts after 7 days of coronary occlusion. Sections from the infarcted area (IA) and the remote non-infarcted area (RA) are shown. Abundant Smad2-expressing periostin+ cells were noted in Smad2 fl/fl infarcts (arrows); in contrast,

very limited Smad2 and periostin colocalization was found in FS2KO hearts (arrows). Arrowheads show the abundance of periostin+ cells that do not express Smad2 in FS2KO animals. B-C: Quantitative analysis shows that FS2KO mice had a marked reduction in the density of periostin+/Smad2+ cells (B) and a lower ratio of Smad2+ positivity in periostin-expressing myofibroblasts (C). Statistical analysis was performed using 2-tailed Student's t-test (****p<0.0001, n=4-5/group). D. After 3 days or coronary occlusion, Smad2 expression was noted in periostin-negative interstitial cells in both Smad2 fl/fl and in FS2KO mice (arrows). Some of these cells may be fibroblasts that have not yet converted to myofibroblasts and do not exhibit Smad2 loss.

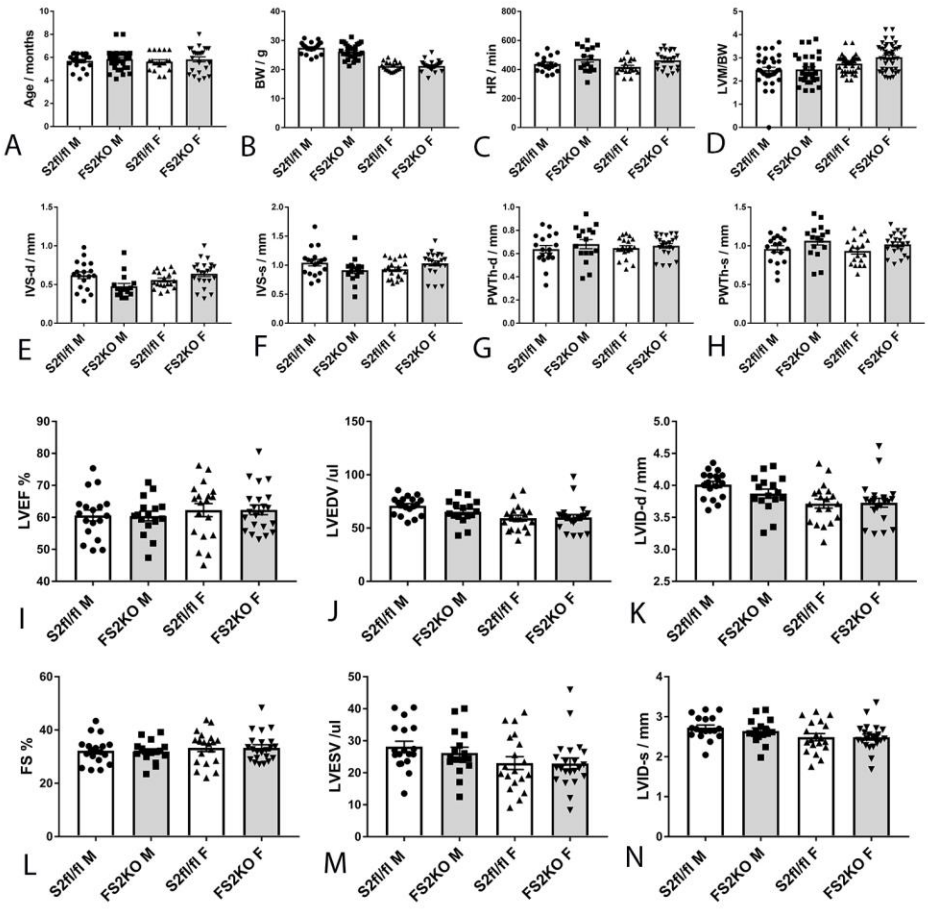


**Supplemental Figure IV**: **Age- and gender-matched Smad2 fl/fl and FS2KO mice had no significant differences in baseline body weight, left ventricular dimensions and function**. Echocardiographic analysis was performed in male (M) and female (F) Smad2 fl/fl and FS2KO mice at 4-6 months of age. Mean age (A) and body weight (B) was not significantly different between groups. Heart rate (C), left ventricular mass (LVM)/body weight(BW) (D), end-diastolic interventricular septum thickness (IVS-d, E), end-systolic

interventricular septum thickness (IVS-s, F), end-diastolic posterior wall thickness (PWThd, G), end-systolic posterior wall thickness (PWThs, H), left ventricular ejection fraction (LVEF, I), fractional shortening (FS, L), left ventricular end-diastolic volume (LVEDV, J), left ventricular end-systolic volume (LVESV, M), left ventricular end-diastolic internal diameter (LVID-d, K), and left ventricular end-systolic internal diameter (LVID-s, N) had no significant differences between Smad2 fl/fl and FS2KO mice, suggesting that loss of Smad2 in activated periostin+ myofibroblasts does not affect baseline cardiac geometry and function (Smad2 fl/fl, M, n=18, F, n=19, FS2KO, M, n=16, F, n=22). Statistical analysis was performed using ANOVA followed by Tukey's multiple comparison test.

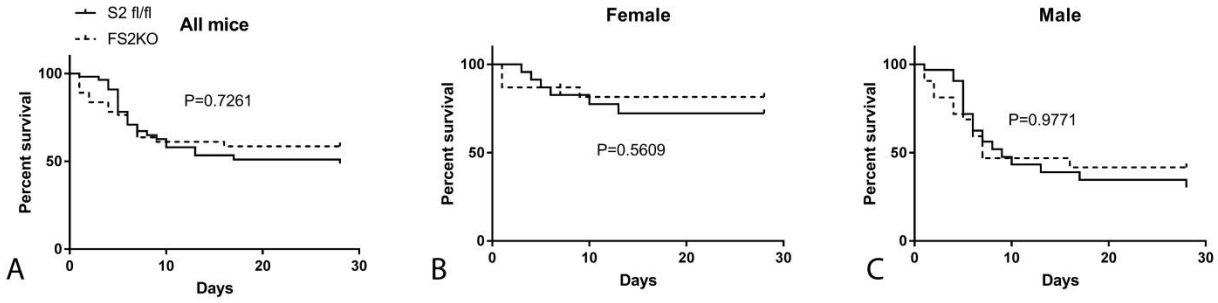


**Supplemental Figure V:** A-C: Female (B) and male (C) FS2KO mice and age-matched Smad2 fl/fl animals exhibited comparable mortality after 28 days of coronary occlusion. Please note the markedly higher mortality in male animals (C) (Smad2 fl/fl, M, n=32, F, n=23, FS2KO, M, n=33, F, n=24). Survival analysis was performed using the Kaplan-Meier method. Mortality was compared using the log rank test.

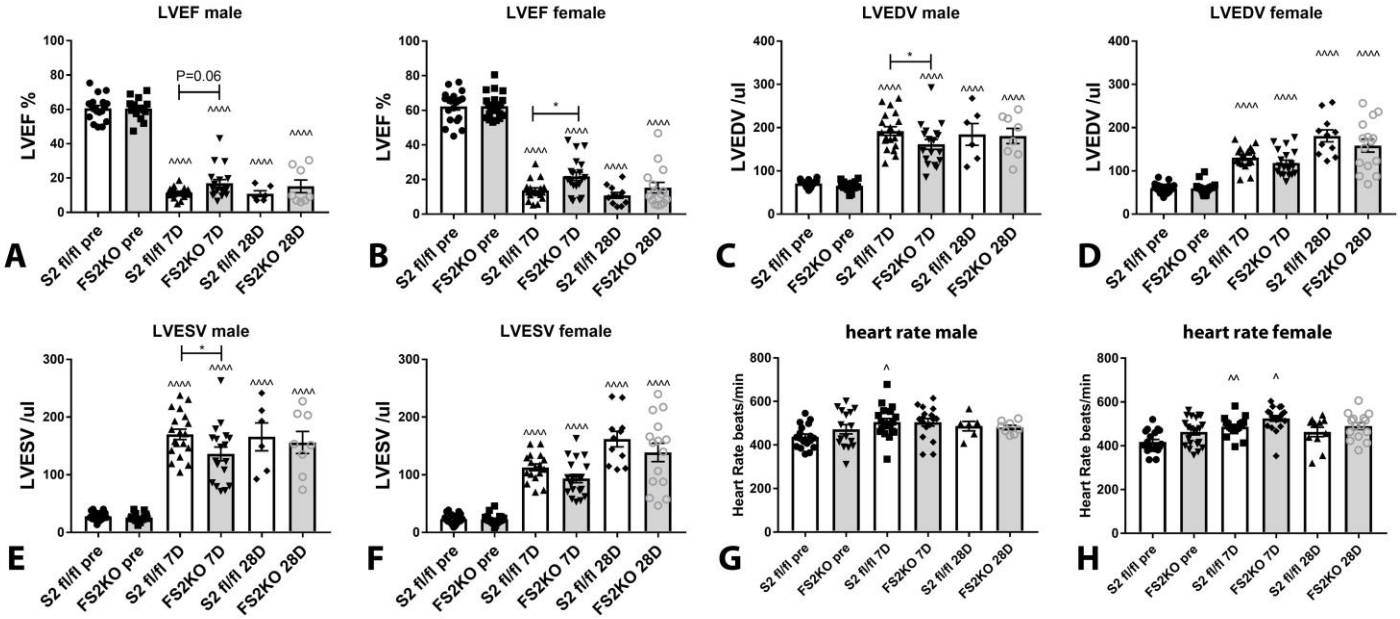


**Supplemental figure VI**: **Effects of myofibroblast-specific Smad2 and Smad3 loss on cardiac function following myocardial infarction in male and female animals.** Gender-specific analysis showed that female FS2KO mice had significantly better systolic function than female Smad2 fl/fl animals (B), whereas male mice exhibited only a trend towards improved function (A). After 28 days of coronary occlusion, no significant differences in ejection fraction were noted between FS2KO mice and Smad2 fl/fl animals in both male and female groups (A-B). LVEDV (C-D) and LVESV (E-F) were significantly lower in male FS2KO mice after 7 days of coronary occlusion, suggesting attenuated dilative remodeling. Female mice had no significant differences (D, F). No significant difference of heart rate was observed between Smad2 fl/fl and FS2KO mice in both genders (G-H). (*p<0.05 vs. S2fl/fl 7D, ^p<0.05, ^^p<0.01, ^^^^p<0.0001 vs. S2fl/fl pre or FS2KO pre - ANOVA followed by Tukey's multiple comparison test) , (pre-echo: Smad2 fl/fl, M, n=18, F, n=19; FS2KO, M, n=16, F, n=22; 7 days echo, Smad2 fl/fl, M, n=19, F, n=17; FS2KO, M, n=18, F, n=19; 28 days echo, Smad2 fl/fl, M, n=6, F, n=11; FS2KO, M, n=8, F, n=15).

.

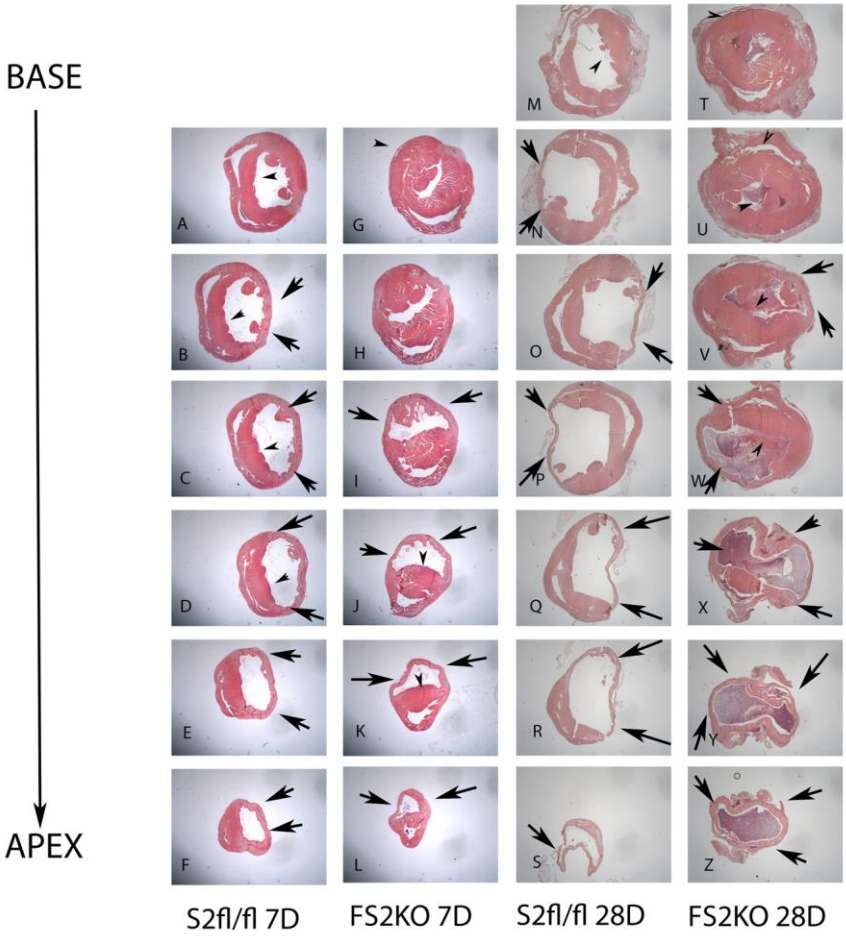


**Supplemental Figure VII: Strategy for morphometric analysis of scar remodeling in infarcted mice.** In order to systematically compare morphometric parameters and scar remodeling between Smad2 fl/fl and FS2KO mice after 7-28 days of permanent coronary occlusion, the infarcted hearts were sectioned from base to apex at 250μm partitions, as previously described[6,8]. 20 sections (5μm each) were cut at each partition; the first section at each level was stained with hematoxylin/eosin (H&E). Areas of replacement fibrosis were identified at each level (arrows). Arrowheads indicate the viable remodeling myocardium. Quantitative analysis of the findings is shown in figure 4. (A-F, Smad2 fl/fl after 7 days of infarction; G-L: FS2KO after 7 days of infarction; M-S: Smad2 fl/fl after 28 days of infarction; T-Z: FS2KO after 28 days of infarction).

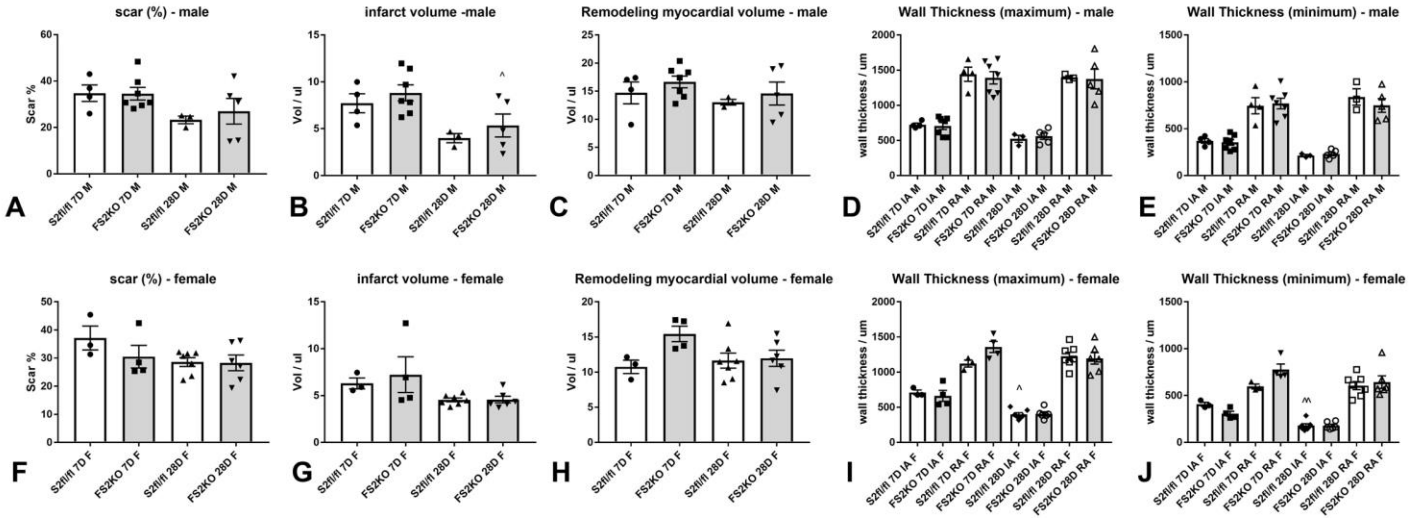


**Supplemental figure VIII**: **Analysis of morphometric parameters in male and female mice**. Scar size (A,F), infarct volume (B,G), the volume of the viable remodeling myocardium (C,H), and the thickness of the infarcted and non-infarcted walls (D-E, I-J) were comparable between FS2KO and Smad2 fl/fl mice in both male and female groups after 7-28 days of coronary occlusion. (^p<0.05, ^^p<0.01, vs. S2fl/fl 7D or FS2KO 7D. S2fl/fl 7D, male, n=4, female, n=3; FS2KO 7D, male, n=7, female, n=4; S2fl/fl 28D, male, n=3, female, n=7; FS2KO 28D, male, n=5, female, n=6. - ANOVA followed by Tukey's multiple comparison test).

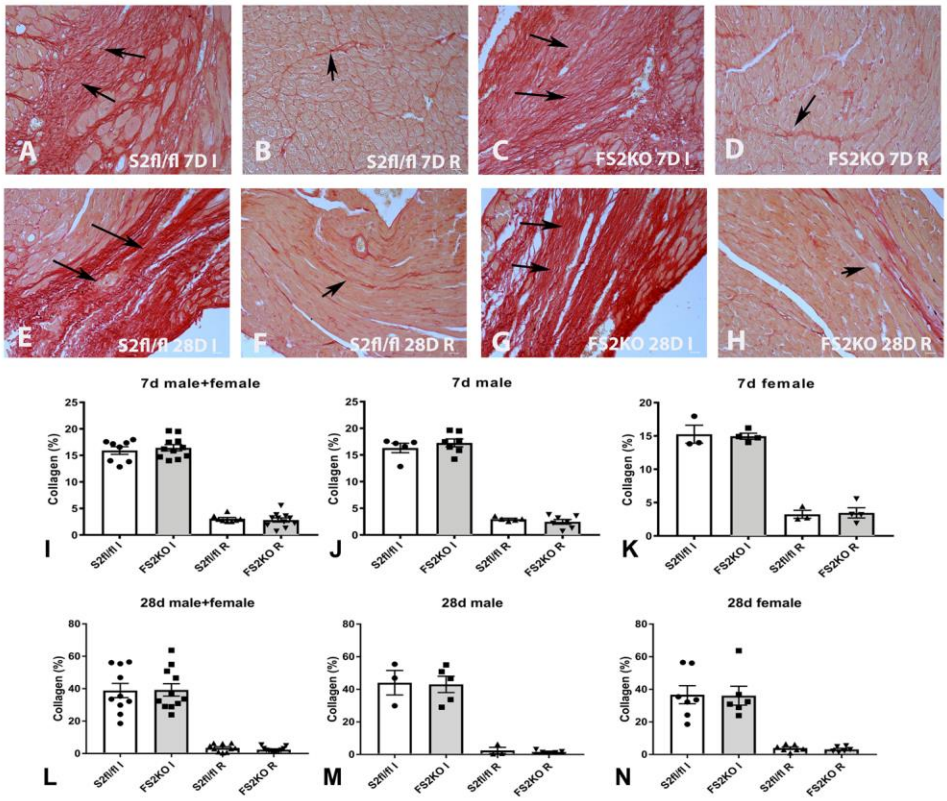


**Supplemental Figure IX: FS2KO mice and Smad2 fl/fl littermates had comparable collagen content in the infarcted area (I) and in the remote remodeling myocardium (R) after 7-28 days of coronary occlusion.** A-H: Collagen staining was performed using picrosirius red; the collagen-stained area was assessed

in infarcted and remodeling areas. Quantitative analysis showed comparable collagen content between Smad2 fl/fl and FS2KO animals in both infarcted and remote remodeling myocardium from male (I-K) and female (L-N) groups after 7-28 days of coronary occlusion. (S2fl/fl 7D, male, n=5, female, n=3; FS2KO 7D, male, n=7, female, n=4; S2fl/fl 28D, male, n=3, female, n=7; FS2KO 28D, male, n=5, female, n=6). Scalebar=20 μm

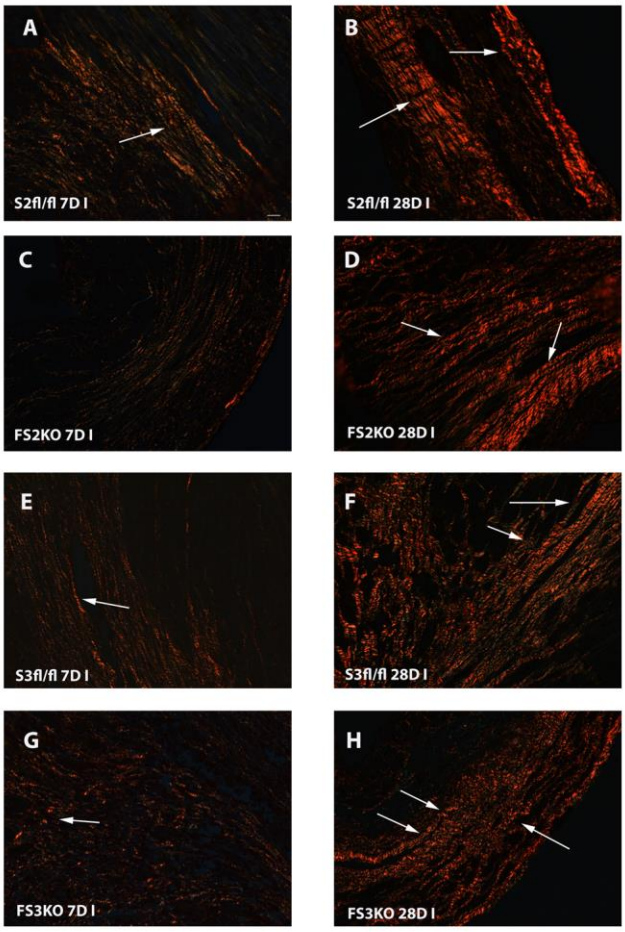


**Supplemental figure X: FS3KO mice, but not FS2KO animals have perturbations of collagen fiber structure after 7 days of coronary occlusion.** Sections from FS2KO, FS3KO, Smad3 fl/fl and Smad2 fl/fl infarcts were stained with with picrosirius red and viewed under polarized light microscopy. Representative images are shown. FS3KO mice had perturbed alignment of collagen fibers and evidence of collagen fragmentation in the infarct zone, when compared to the well-aligned fibers in S3 fl/fl infarcts (E-H, arrows). In contrast, FS2KO mice had a well-organized network of collagen fibers in the infarcted heart at both 7 and 28 day timepoints (A-D, arrows). Scalebar=20 μm

.

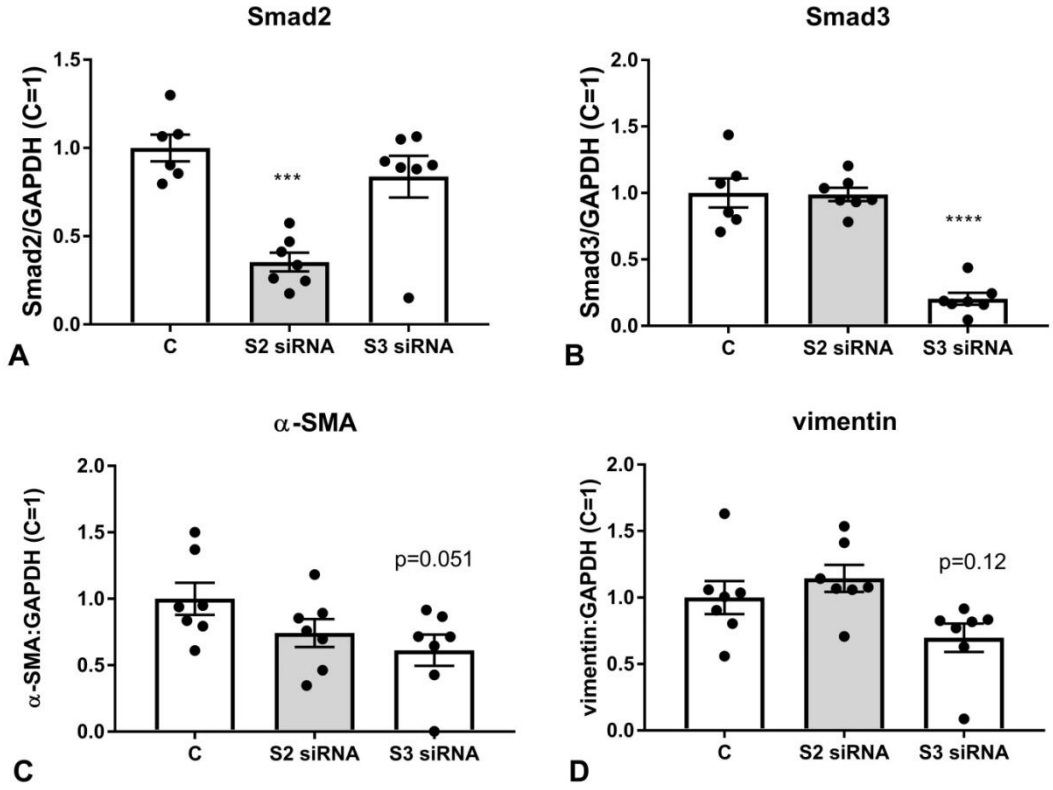


**Supplemental Figure XI**: Effects of Smad3 and Smad2 siRNA KD on α-SMA and vimentin gene expression in cardiac fibroblasts cultured in plates. A-B: Effectiveness and specificity of the siRNA KD strategy was assessed. Smad2, but not Smad3 siRNA KD markedly reduced Smad2 levels. B: Smad3, but not Smad2 siRNA KD decreased Smad3 expression (C, control siRNA). C: Smad3 KD cells had trends towards reduced α-SMA expression (p=0.051) and vimentin expression (p=0.12). In contrast, Smad2 KD did not affect α-SMA and vimentin levels (***p<0.001, ****p<0.0001 vs C, n=6-7/group - ANOVA followed by Tukey's multiple comparison test).

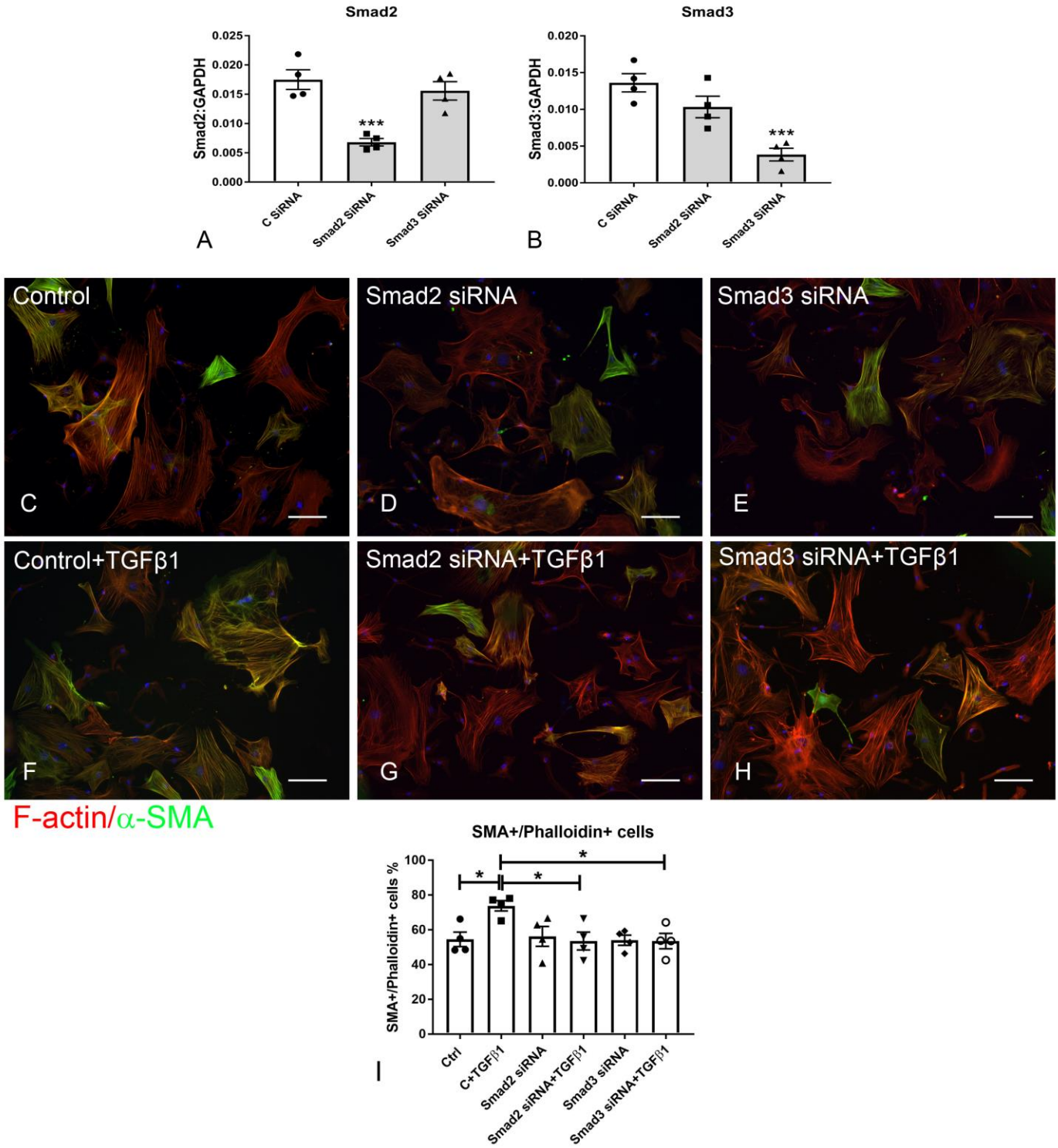


**Supplemental figure XII: Smad2 or Smad3 knockdown attenuate α-SMA incorporation into stress fibers in TGF-β-stimulated fibroblasts**. A-B: Effectiveness and specificity of Smad2 (A) and Smad3 (B) siRNA KD in fibroblasts was demonstrated using qPCR. Smad2 KD reduced Smad2 levels without affecting Smad3 levels, whereas Smad3 KD attenuated Smad3 synthesis without significant effects on Smad2 expression. C-H: Dual fluorescence with phalloidin-AF594 and a FITC-labeled anti-α-SMA antibody showed that Smad2 or Smad3

KD attenuated formation of α-SMA-decorated stress fibers in TGF-β-stimulated fibroblasts (C-H). Quantitative analysis showed that Smad2 and Smad3 KD did not affect the percentage of α-SMA+ cells at baseline (C-E, I), but significantly reduced the number of α-SMA+ cells following stimulation with TGF-β1 (F-H, I). (*$p<0.05$, n=4/group - ANOVA followed by Tukey's multiple comparison test).

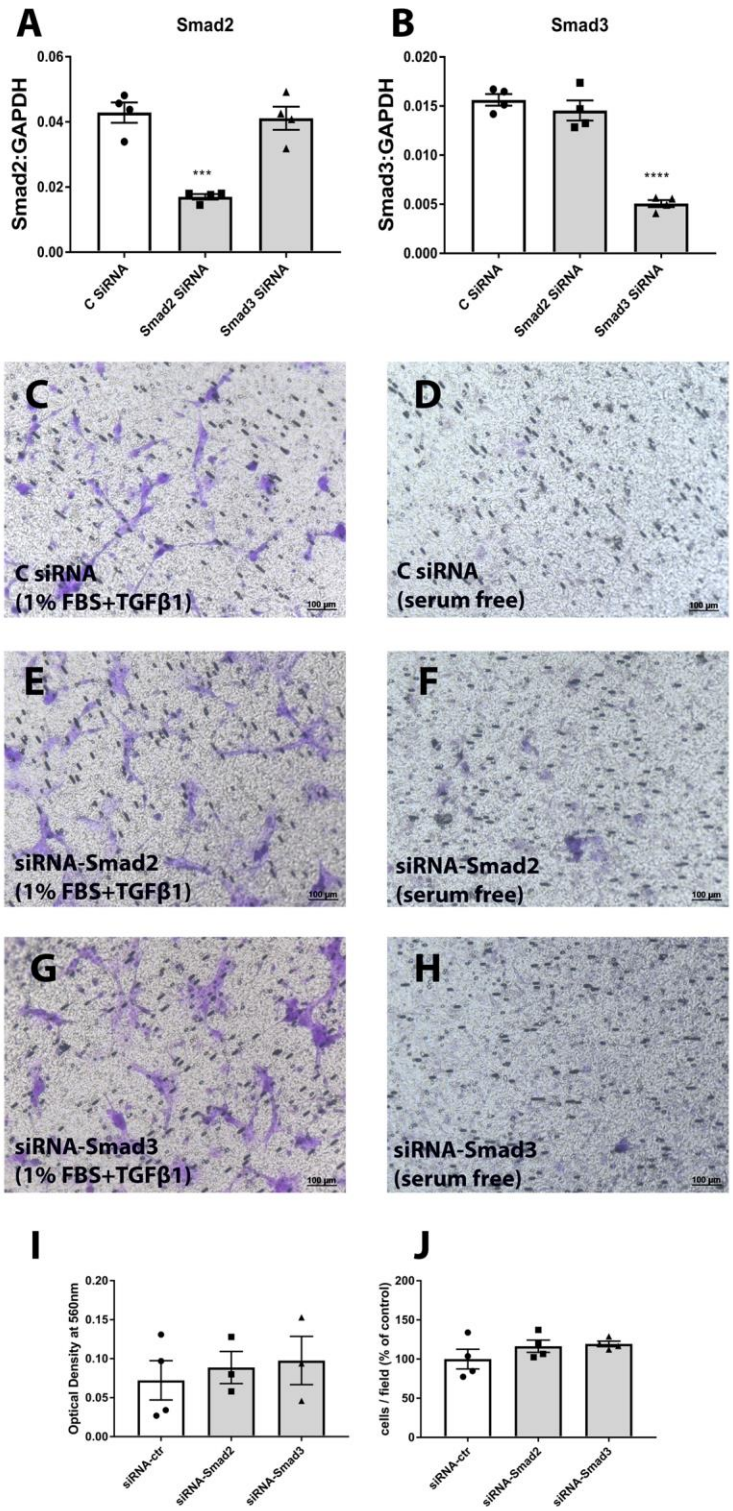


**Supplemental figure XIII: Effects of Smad2 and Smad3 loss on migration of fibroblasts in response to serum and TGF-β1.** qPCR was used to document Smad2 and Smad3 loss following siRNA knockdown (A-B). A transwell assay was used to study the role of Smad2 and Smad3 in fibroblast migration in response to serum and TGF-β1. Representative images of fibroblasts treated with control siRNA (C-D), Smad2 siRNA (E-F), Smad3 siRNA (G-H) that migrate towards serum free DMEM/F12 or 1% FBS DMEM/F12 +20ng/ml TGF-β1

are shown. In the serum-free chambers, there was very limited fibroblast migration (D, F, H). Stimulation with serum (1% FBS) and TGF-β1 (20ng/ml) induced significant cardiac fibroblast migration (C, E, G). Quantitative analysis demonstrated that Smad2 or Smad3 siRNA knockdown had no significant effects on fibroblast migration (I-J). (n=4/group - ANOVA followed by Tukey's multiple comparison test).

.

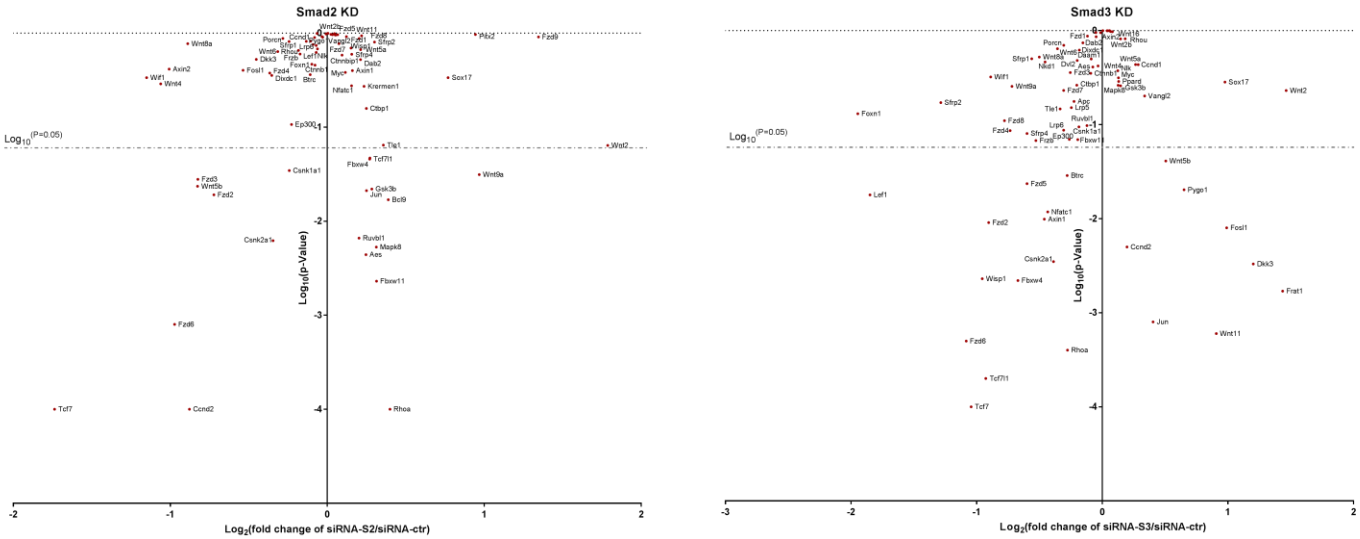


**Supplemental figure XIV**: This volcano plot summarizes planar cell polarity pathways (PCP) genes expression in isolated fibroblasts treated with Smad2 siRNA (left panel) or Smad3 siRNA (right panel), compared to control siRNA. Detailed data are provided in Supplementary Table I. Statistical analysis was performed using ANOVA followed by Tukey's multiple comparison test.

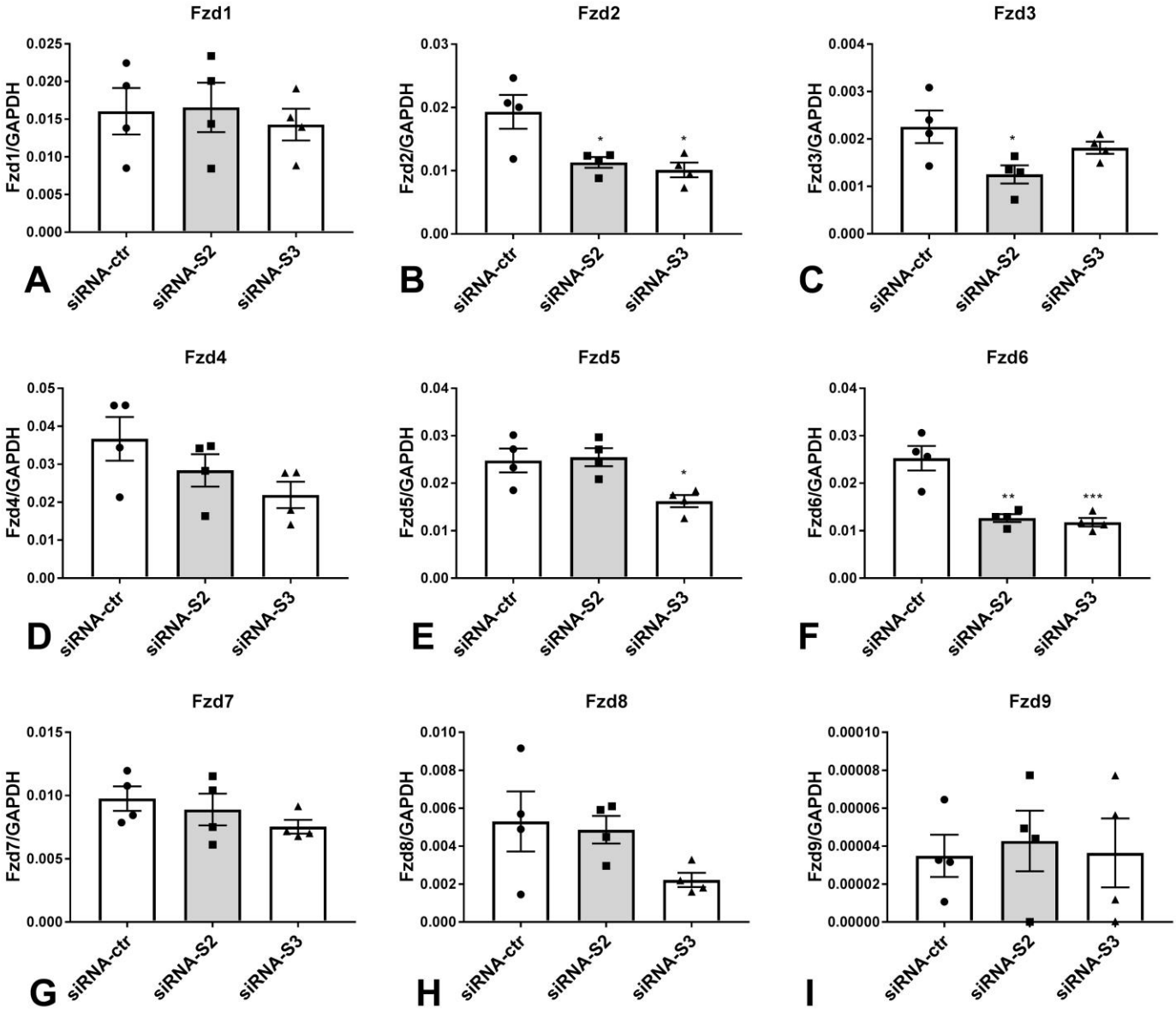


**Supplemental figure XV: Effects of Smad2 and Smad3 loss on frizzled (Fzd) gene expression in cardiac fibroblasts.** Frizzled genes are critically involved in PCP pathway signaling; expression of Fzd2 has been observed in polarized infarct myofibroblasts[12] and may be involved in cell alignment in healing infarcts. Neither Smad2 nor Smad3 KD affected Fzd1 expression in cardiac fibroblasts (A). Fzd2 (B) and Fzd6 (F) mRNA levels were significantly reduced in both Smad2 and Smad3 KD cells. Smad2 KD reduced Fzd3 expression (C), whereas Smad3 KD decreased Fzd5 (E) levels. Expression of Fzd4 (D), Fzd7 (G), Fzd8 (H) and Fzd9 (I) was not affected by Smad3 or Smad2 loss (*$p<0.05$, **$p<0.01$, ***$p<0.001$ vs. control siRNA, n=4/group - ANOVA followed by Tukey's multiple comparison test).

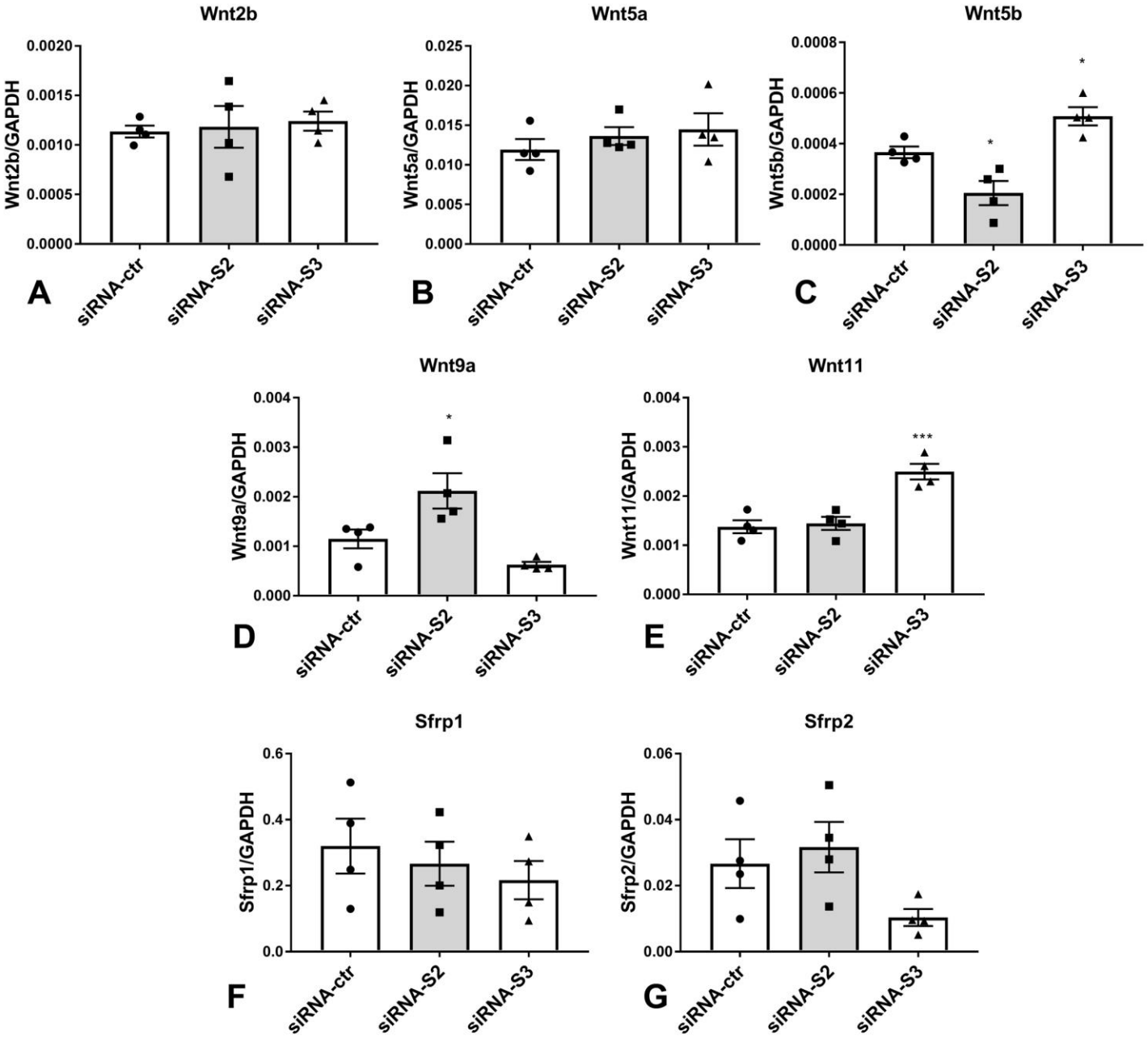


**Supplemental figure XVI: Effects of Smad2 and Smad3 KD on Wnt and Sfrp gene expression in cardiac fibroblasts.** Wnt5b expression was significantly decreased in Smad2 KD fibroblasts, but increased in Smad3 KD cells (C). Moreover, Smad2 KD increased Wnt9a levels (D), whereas Smad3 KD accentuated Wnt11 expression (E). Expression of Wnt2b (A), Wnt5a (B) was not affected by Smad2 or Samd3 loss. Cardiac fibroblasts also expressed high levels of the secreted frizzle-related proteins Sfrp1 and Sfrp2. However, Sfrp1 (F) and Sfrp2 (G) were not affected by Smad2 or Smad3 KD (*$p<0.05$, ***$p<0.001$, n=4/group - ANOVA followed by Tukey's multiple comparison test)

**SUPPLEMENTARY TABLES:**

**Supplemental Table 1:** Effects of Smad2 and Smad3 siRNA knockdown on the expression of Wnt signaling pathway genes by cardiac fibroblasts.

| Gene name | Gene symbols | Smad2 siRNA | | Smad3 siRNA | |
|---|---|---|---|---|---|
| | | Fold change vs. control siRNA | ***P*** | Fold change vs. control siRNA | ***P*** |
| Amino-terminal enhancer of split | *Aes* | 1.19 | 0.0044† | 0.95 | 0.4101 |
| Adenomatosis polyposis coli | *Apc* | 1.05 | 0.7736 | 0.86 | 0.1765 |
| Axin1 | *Axin1* | 1.12 | 0.3998 | 0.73 | 0.0099† |
| Axin2 | *Axin2* | 0.50 | 0.4144 | 0.96 | 0.9518 |
| B-cell CLL/lymphoma 9 | *Bcl9* | 1.31 | 0.0169† | 0.97 | 0.8598 |
| Beta-transducin repeat containing protein (b-TrCP) | *Btrc* | 0.93 | 0.3616 | 0.82 | 0.0288† |
| Cyclin D1 | *Ccnd1* | 0.93 | 0.8228 | 1.22 | 0.4349 |
| Cyclin D2 | *Ccnd2* | 0.54 | 0.0001† | 1.15 | 0.0050† |
| Casein kinase 1, alpha 1 | *Csnk1a1* | 0.85 | 0.0346† | 0.88 | 0.0946† |
| Casein kinase 2, alpha 1 polypeptide | *Csnk2a1* | 0.79 | 0.0062† | 0.76 | 0.0035† |
| C-terminal binding protein 1 | *Ctbp1* | 1.19 | 0.1582 | 0.87 | 0.2626 |

| | | | | | |
|---|---|---|---|---|---|
| Catenin (Cadherin associated protein), beta1 | *Ctnnb1* | 0.95 | 0.457 | 0.94 | 0.3512 |
| Catenin beta interacting protein 1 | *Ctnnbip1* | 1.07 | 0.5838 | 0.99 | 0.9496 |
| Dishevelled associated activator of morphogenesis 1 | *Daam1* | 0.99 | 0.9799 | 0.94 | 0.4994 |
| Disabled homolog 2 (Drosophila) | *Dab2* | 1.16 | 0.5227 | 0.90 | 0.7409 |
| DIX domain containing 1 | *Dixdc1* | 0.78 | 0.3555 | 0.88 | 0.6205 |
| Dickkopf homolog 1 (Xenopus laevis) | *Dkk1* | ND | - | ND | - |
| Dickkopf homolog 3 (Xenopus laevis) | *Dkk3* | 0.73 | 0.5255 | 2.30 | 0.0033† |
| Dishevelled, dsh homolog 1 (Dorsophila) | *Dvl1* | 1.02 | 0.9709 | 1.00 | 0.9994 |
| Dishevelled 2, dsh homolog (Dorsophila) | *Dvl2* | 0.95 | 0.8992 | 0.87 | 0.4805 |
| E1A binding protein p300 | *Ep300* | 0.85 | 0.1068 | 0.83 | 0.0697 |
| F-box and WD-40 domain protein 11 | *Fbxw11* | 1.24 | 0.0023† | 0.87 | 0.0693 |
| F-box and WD-40 domain protein 4 | *Fbxw4* | 1.21 | 0.0469† | 0.63 | 0.0022† |
| Fibroblast growth factor 4 | *Fgf4* | ND | - | ND | - |

| | | | | | |
|---|---|---|---|---|---|
| Fos-like antigen 1 | *Fosl1* | 0.69 | 0.4024 | 1.99 | 0.0080† |
| Forkhead box N1 | *Foxn1* | 0.93 | 0.4672 | 0.26 | 0.1307 |
| Frequently rearranged in advanced T-cell lymphomas | *Frat1* | 1.15 | 0.8768 | 2.70 | 0.0017† |
| Frizzled-related protein | *Frzb* | 0.89 | 0.5987 | 0.69 | 0.0677 |
| Frizzled homolog 1 (Drosophila) | *Fzd1* | 1.03 | 0.9885 | 0.92 | 0.8735 |
| Frizzled homolog 2 (Drosophila) | *Fzd2* | 0.61 | 0.0191† | 0.53 | 0.0091† |
| Frizzled homolog 3 (Drosophila) | *Fzd3* | 0.56 | 0.0279† | 0.84 | 0.3583 |
| Frizzled homolog 4 (Drosophila) | *Fzd4* | 0.78 | 0.3764 | 0.60 | 0.0865 |
| Frizzled homolog 5 (Drosophila) | *Fzd5* | 1.04 | 0.9552 | 0.66 | 0.0236† |
| Frizzled homolog 6 (Drosophila) | *Fzd6* | 0.51 | 0.0008† | 0.47 | 0.0005† |
| Frizzled homolog 7 (Drosophila) | *Fzd7* | 0.94 | 0.7573 | 0.81 | 0.2311 |
| Frizzled homolog 8 (Drosophila) | *Fzd8* | 1.16 | 0.9367 | 0.58 | 0.1101 |
| Frizzled homolog 9 (Drosophila) | *Fzd9* | 2.54 | 0.9104 | 1.03 | 0.9961 |
| Glycogen synthase kinase 3 beta | *Gsk3b* | 1.22 | 0.0220† | 1.11 | 0.2588 |
| Jun oncogene | *Jun* | 1.19 | 0.0211† | 1.32 | 0.0008† |

| | | | | | |
|---|---|---|---|---|---|
| Kringle containing transmembrane protein 1 | *Krermen1* | 1.18 | 0.2718 | 1.03 | 0.9971 |
| Lymphoid enhancer binding factor 1 | *Lef1* | 0.95 | 0.6228 | 0.28 | 0.0179† |
| Low density lipoprotein receptor-related protein 5 | *Lrp5* | 0.98 | 0.9190 | 0.84 | 0.1516 |
| Low density lipoprotein receptor-related protein 5 | *Lrp6* | 0.95 | 0.7395 | 0.81 | 0.0872 |
| Mitogen-activated protein kinase 8 | *Mapk8* | 1.24 | 0.0053† | 1.09 | 0.2618 |
| Matrix metallopeptidase 7 | *Mmp7* | ND | - | ND | - |
| Myelocytomatosis oncogene | *Myc* | 1.08 | 0.3826 | 1.09 | 0.3147 |
| Nuclear factor of activated T-cells, cytoplasmic, calcineurin-dependent 1 | *Nfatc1* | 1.11 | 0.2757 | 0.74 | 0.0118† |
| Naked cuticle 1 homolog (Dorsophila) | *Nkd1* | 0.96 | 0.9934 | 0.73 | 0.4641 |
| Nemo like kinase | *Nlk* | 0.96 | 0.6795 | 1.09 | 0.3740 |
| Paired-like homeodomain transcription factor 2 | *Pitx2* | 1.92 | 0.9668 | 1.05 | 0.9785 |
| Porcupine homolog (Dorsophila) | *Porcn* | 0.82 | 0.8785 | 0.81 | 0.6971 |

| | | | | | |
|---|---|---|---|---|---|
| Peroxisome proliferator activator receptor delta | *Ppard* | 1.00 | 0.9971 | 1.09 | 0.2880 |
| Prickle homolog 1 (Dorsophila) | *Prickle1* | 1.02 | 0.9617 | 1.06 | 0.9731 |
| Pygopus 1 | *Pygo1* | 0.91 | 0.8192 | 1.57 | 0.0203† |
| Ras homolog gene family , member A | *Rhoa* | 1.32 | 0.0001† | 0.83 | 0.0004† |
| Ras homolog gene family , member U | *Rhou* | 0.88 | 0.6545 | 1.13 | 0.8186 |
| Ruvb-like protein 1 | *Ruvbl1* | 1.15 | 0.0066† | 0.92 | 0.0977 |
| Secreted frizzled-related protein 1 | *Sfrp1* | 0.84 | 0.8148 | 0.68 | 0.5012 |
| Secreted frizzled-related protein 2 | *Sfrp2* | 1.23 | 0.8035 | 0.41 | 0.1715 |
| Secreted frizzled-related protein 4 | *Sfrp4* | 1.11 | 0.5959 | 0.66 | 0.0804 |
| SRY-box containning gene 17 | *Sox17* | 1.70 | 0.3362 | 1.97 | 0.2832 |
| Transcription factor 7, T-cell specific | *Tcf7* | 0.30 | 0.0001† | 0.48 | 0.0001† |
| Transcription factor 7-like 1, (T-cell specific, MHG box) | *Tcf7l1* | 1.21 | 0.0457† | 0.53 | 0.0002† |
| Transducin-like enhancer of split 1, homolog of Drosophila E (spl) | *Tle1* | 1.28 | 0.0645 | 0.79 | 0.1469 |
| Vang-like 2 (van gogh, Dorsophila) | *Vangl2* | 0.98 | 0.9055 | 1.26 | 0.2020 |

| | | | | | |
|---|---|---|---|---|---|
| Wnt1 inhibitory factor 1 | *Wif1* | 0.45 | 0.3363 | 0.54 | 0.3219 |
| WNT1 inducible signaling pathway protein 1 | *Wisp1* | 1.11 | 0.6937 | 0.52 | 0.0023† |
| Wingless-related MMTV integration site 1 | *Wnt1* | ND | - | ND | - |
| Wingless-related MMTV integration site 10a | *Wnt10a* | ND | - | ND | - |
| Wingless-related MMTV integration site 11 | *Wnt11* | 1.09 | 0.9187 | 1.88 | 0.0006† |
| Wingless-related MMTV integration site 16 | *Wnt16* | 1.05 | 0.9640 | 1.04 | 0.9994 |
| Wingless-related MMTV integration site 2 | *Wnt2* | 3.45 | 0.0640 | 2.76 | 0.2303 |
| Wingless-related MMTV integration site 2b | *Wnt2b* | 1.04 | 0.9582 | 1.11 | 0.8166 |
| Wingless-related MMTV integration site 3 | *Wnt3* | ND | - | ND | - |
| Wingless-related MMTV integration site 3a | *Wnt3a* | ND | - | ND | - |
| Wingless-related MMTV integration site 4 | *Wnt4* | 0.48 | 0.2891 | 0.98 | 0.4207 |
| Wingless-related MMTV integration site 5a | *Wnt5a* | 1.16 | 0.6667 | 1.20 | 0.4360 |
| Wingless-related MMTV integration site 5b | *Wnt5b* | 0.56 | 0.0235† | 1.42 | 0.0411† |

| | | | | | |
|---|---|---|---|---|---|
| Wingless-related MMTV integration site 6 | *Wnt6* | 0.80 | 0.6363 | 0.78 | 0.6420 |
| Wingless-related MMTV integration site 7a | *Wnt7a* | ND | - | ND | - |
| Wingless-related MMTV integration site 7b | *Wnt7b* | ND | - | ND | - |
| Wingless-related MMTV integration site 8a | *Wnt8a* | 0.54 | 0.7731 | 0.71 | 0.5225 |
| Wingless-related MMTV integration site 8b | *Wnt8b* | ND | - | ND | - |
| Wingless-related MMTV integration site 9a | *Wnt9a* | 1.96 | 0.0313† | 0.61 | 0.2553 |

†P value <0.05, n=4/group.

ND-Not Detected

SUPPLEMENTAL REFERENCES:


1. Lindsley A, Snider P, Zhou H, Rogers R, Wang J, Olaopa M, Kruzynska-Frejtag A, Koushik SV, Lilly B, Burch JB, Firulli AB Conway SJ. Identification and characterization of a novel Schwann and outflow tract endocardial cushion lineage-restricted periostin enhancer. *Dev Biol* 2007;**307**:340-355.
2. Takeda N, Manabe I, Uchino Y, Eguchi K, Matsumoto S, Nishimura S, Shindo T, Sano M, Otsu K, Snider P, Conway SJ Nagai R. Cardiac fibroblasts are essential for the adaptive response of the murine heart to pressure overload. *J Clin Invest* 2010;**120**:254-265.
3. Conway SJ Molkentin JD. Periostin as a heterofunctional regulator of cardiac development and disease. *Curr Genomics* 2008;**9**:548-555.
4. Kong P, Christia P, Saxena A, Su Y Frangogiannis NG. Lack of specificity of fibroblast-specific protein 1 in cardiac remodeling and fibrosis. *Am J Physiol Heart Circ Physiol* 2013;**305**:H1363-1372.
5. Oka T, Xu J, Kaiser RA, Melendez J, Hambleton M, Sargent MA, Lorts A, Brunskill EW, Dorn GW, 2nd, Conway SJ, Aronow BJ, Robbins J Molkentin JD. Genetic manipulation of periostin expression reveals a role in cardiac hypertrophy and ventricular remodeling. *Circ Res* 2007;**101**:313-321.
6. Kong P, Shinde AV, Su Y, Russo I, Chen B, Saxena A, Conway SJ, Graff JM Frangogiannis NG. Opposing Actions of Fibroblast and Cardiomyocyte Smad3 Signaling in the Infarcted Myocardium. *Circulation* 2018;**137**:707-724.
7. Dobaczewski M, Xia Y, Bujak M, Gonzalez-Quesada C Frangogiannis NG. CCR5 signaling suppresses inflammation and reduces adverse remodeling of the infarcted heart, mediating recruitment of regulatory T cells. *Am J Pathol* 2010;**176**:2177-2187.
8. Christia P, Bujak M, Gonzalez-Quesada C, Chen W, Dobaczewski M, Reddy A Frangogiannis NG. Systematic characterization of myocardial inflammation, repair, and remodeling in a mouse model of reperfused myocardial infarction. *J Histochem Cytochem* 2013;**61**:555-570.
9. Bujak M, Ren G, Kweon HJ, Dobaczewski M, Reddy A, Taffet G, Wang XF Frangogiannis NG. Essential Role of Smad3 in Infarct Healing and in the Pathogenesis of Cardiac Remodeling. *Circulation* 2007;**116**:2127-2138.
10. Bujak M, Dobaczewski M, Gonzalez-Quesada C, Xia Y, Leucker T, Zymek P, Veeranna V, Tager AM, Luster AD Frangogiannis NG. Induction of the CXC chemokine interferon-gamma-inducible protein 10 regulates the reparative response following myocardial infarction. *Circ Res* 2009;**105**:973-983.
11. Biernacka A, Cavalera M, Wang J, Russo I, Shinde A, Kong P, Gonzalez-Quesada C, Rai V, Dobaczewski M, Lee DW, Wang XF Frangogiannis NG. Smad3 Signaling Promotes Fibrosis While Preserving Cardiac and Aortic Geometry in Obese Diabetic Mice. *Circ Heart Fail* 2015;**8**:788-798.
12. Blankesteijn WM, Essers-Janssen YP, Verluyten MJ, Daemen MJ Smits JF. A homologue of Drosophila tissue polarity gene frizzled is expressed in migrating myofibroblasts in the infarcted rat heart. *Nat Med* 1997;**3**:541-544.